Folly Abevi
Research and Product Development Engineer,
SKF Transrol,
148 Rue Felix Esclangon,
Chambéry 73000, France
e-mail: folly.abevi@skf.com

Alain Daidie
Institut Clément ADER,
INSA (Institut National des Sciences Appliquées),
Université de Toulouse,
3 Rue Caroline Aigle,
Toulouse 31400, France
e-mail: alain.daidie@insa-toulouse.fr

Michel Chaussumier
Institut Clément ADER,
INSA (Institut National des Sciences Appliquées),
Université de Toulouse,
3 Rue Caroline Aigle,
Toulouse 31400, France
e-mail: michel.chaussumier@insa-toulouse.fr

Marc Sartor
Institut Clément ADER,
INSA (Institut National des Sciences Appliquées),
Université de Toulouse,
3 Rue Caroline Aigle,
Toulouse 31400, France
e-mail: marc.sartor@insa-toulouse.fr

Static Load Distribution and Axial Stiffness in a Planetary Roller Screw Mechanism

In this paper, an original approach is proposed to calculate the static load distribution and the axial stiffness of a planetary roller screw (PRS) mechanism. Assuming that the external loading is shared equally over an arbitrary number of rollers, only a sector of the system is represented to save on computing time. The approach consists in using a structure of bars, beams, and nonlinear springs to model the different components of the mechanism and their interactions. This nonlinear model describes the details of the mechanism and captures the shape of the nut as well as the bending deformation of the roller. All materials are assumed to operate in the elastic range. The load distribution and the axial stiffness are determined in three specific configurations of the system for both compressive and tensile loads. Further, the influence of the shape of the nut is studied in the case of the inverted PRS. The results obtained from this approach are also compared to those computed with a three-dimensional finite-element (3D FE) model. Finally, since the calculations appear to be very accurate, a parametric study is conducted to show the impact of the bending of the roller on the load distribution. [DOI: 10.1115/1.4031859]

Keywords: planetary roller screw, inverted, load distribution, load sharing, axial stiffness, finite element, model, bar, beam, nonlinear spring, bending deformation

1 Introduction

The PRS is a mechanism that transmits heavy loads with extremely high precision and low friction, by converting a rotary motion into a linear motion and vice versa. In the past decade, it has become the object of increasing interest due to new challenges in industrial fields and mainly in aeronautics. As it can be involved in electromechanical actuators designed for electric aircraft, many projects are focusing on improving knowledge of the mechanism. In the PRS, the load is transmitted through multiple contacting points at each side of the rollers, and the way the external load is shared over those points is of great importance for the proper sizing of this mechanism. As it is not uniform and involves large numbers of parameters and nonlinear contacts, determining the load distribution is not easy.

Earlier work in the literature put more emphasis on the practical and experimental aspects of the PRS, such as the apparent coefficient of friction [1], the static stiffness and vibration frequencies [2], the efficiency and failure modes [3], the elastic elements in the preloaded PRS [4], and the limitations in terms of force, slip, and lead properties [5] of the mechanism. Few, but recent, papers have raised and dealt with the theoretical and fundamental aspects of PRSs to provide a common theory and to support engineering applications. Velinsky et al. [6] analyzed the kinematics, the efficiency, and the load carrying capacity of the roller screw mechanism. His kinematic analysis took the axial and angular motions of the roller into account. He also developed a slip pattern between the contacting threaded components and showed that slip always occurred in the system. The load carrying capacity was derived on the basis of geometric and equilibrium conditions. Jones and Velinsky [7] provided a kinematic model to predict the axial migration of the rollers relative to the nut in the PRS mechanism, which is due to manufacturing errors. He explained that this migration is caused by slip at the nut–roller interface, which in turn is caused by a pitch mismatch between the spur-ring gear and the effective nut–roller helical gear pairs. This migration causes bending of the teeth and can lead to failure of the system. Later, using the principle of conjugate surfaces, Jones and Velinsky [8] developed a model to accurately determine the components' radii in order to help reduce the phenomenon of roller migration. Liu and Wang [9] attempted to describe the structure and movement principle of the PRS and established the equation of screw and roller thread surfaces generated by straight profiles. Shangjun et al. [10] proposed a numerical approach to minimize the meshing clearance in a PRS.

However, as far as the load sharing issue is concerned, few researchers have proposed models for its computation in the PRS. Shangjun et al. [11] studied the relationships among parameters and suggested a model to determine the static load distribution within the PRS. Derived from those of ball screws [12], the model is based on the equilibrium condition and the elastic relations between the screw and the nut. The rollers are assumed to be rigid bodies and only their contacting deformations at the nut–roller and screw–roller interfaces are involved in the calculations, which are based on Hertzian theory. Rys and Lisowski [13] proposed an analytical model to calculate the load distribution in static situations. Their model was intended for preliminary design purposes. The model was based upon the deformations of the rolling elements considered as deformations of rectangular volumes subjected to shear stress. However, Rys's model is not able to guarantee that the value passing through the first active thread is really correct. Recently, Jones and Velinsky [14] used a direct stiffness method to model the whole PRS as a large spring composed of individual linear and linearized springs that reflect the

Contributed by the Mechanisms and Robotics Committee of ASME for publication in the JOURNAL OF MECHANICAL DESIGN. Manuscript received May 11, 2015; final manuscript received September 27, 2015; published online November 16, 2015. Assoc. Editor: Ettore Pennestri.

various compliances. They used their method to compute the axial stiffness and the load distribution at each side of a roller in four different loading configurations. They also studied the sensitivity of their model to the number of threads and rollers.

The results obtained by the previous three authors show that the load distribution is not uniform at each side of a roller in a PRS. Their models did not involve the flange of the nut and only that of Jones and Velinsky involved the elasticity of the roller and the axial deformation of threads. It can also be noted that the load distribution is a very new topic in the literature and poses a particular set of problems. Earlier models did not consider the bending flexibility of the roller or even the shape of the nut, which can have a significant impact on the load distribution and the axial and radial stiffnesses. Neither the axial relative position of the roller, defining the configuration of the system, nor the boundary conditions (BCs) on the component were fully analyzed. An efficient model must take these parameters into account to ensure realistic load distributions at the nut and the screw sides of the roller. In a prior work, using 3D FE analysis, Abevi [15] demonstrated that the load distribution, in the case of an "inverted" PRS was not the same at each side of the roller regarding the threads of the roller in contact with the nut and the screw, respectively. Among other things, he provided a model to calculate the contact radii and the curvatures of contacting surfaces accurately in an inverted PRS.

This paper presents a fast, robust method based on a hybrid model of one-dimensional finite-elements (1D FEs) and nonlinear springs to compute the axial stiffness and the static load distribution in any type of PRS. In the current investigations, only the shape of the nut and the bending flexibility of the roller are taken into account. For the sake of simplicity, other parameters such as the thread deformations (bending deformation, shrinkage deformation, shear deformation, etc.) and the radial expansion of the nut are neglected and will be investigated in a future work. The load distribution is determined in three specific configurations of the system, taking cases of both compressive and tensile loading. The results obtained from this approach are also compared to reference numerical results. The approach developed here is used to study the load distribution in an inverted PRS through a parametric analysis based on the variation of the external load.

2 Inverted PRS

There are two kinds of nonrecirculating PRS: the standard and the inverted PRS (Fig. 1). For the standard one, the rollers are equally distributed circumferentially within the nut and the ring gears, as well as the guiding rings, are mounted inside the nut. Theoretically, there is no slip between the rollers and the nut. In contrast, more compact and more capacitive, the inverted PRS has its rollers set circumferentially around the screw shaft with the guiding rings and the ring gears. Theoretically, there is no slip between the rollers and the screw shaft. The nut of the inverted PRS studied has two flanges (Fig. 2), which are connected to the bearings of the supports. A static 3D FE analysis was previously carried out to investigate the in-depth stresses, pressure distribution, and deflection results that contribute to the calculation of the load distribution and the axial stiffness. These results will be considered as reference data in the following and used for comparison.

3 Model of the Static Load Distribution

3.1 The Problem. Since there are two types of contacts for the roller, with different load distributions, it is necessary to describe them precisely. Here, the teeth of the gearing are assumed not to deflect during axial loading and are not taken into consideration in the current model.

Let us denote the axial external force acting upon the central screw shaft by F. This force is assumed to be known in direction and strength. Similarly, we denote the normal force acting on a contact C_v by F_v. F_v is an unknown variable that has to be determined using a relevant model. Because of the static equilibrium, it is possible to write the following relation, Eq. (1), according to the nut or the screw:

$$\frac{F}{n_r} = \sum_{v=1}^{N_c} F_v.(\cos\alpha_{nv}.\cos\beta_v - \mu_v.\sin\beta_v) = \sum_{v=1}^{N_c} F_v.\cos(\psi_v) \quad (1)$$

where $\boldsymbol{v}$ is a generalized parameter such as $v \in \{k, g\}$ with k and g referring to the screw–roller and the nut–roller contacts, respectively, β_v is the helix angle related to the contact C_v, α_{nv} is the normal pressure related to the contact C_v, and μ_v is the coefficient of friction related to contact C_v. N_c is the number of contacts at each side of the roller. The parameter ψ_v is a generalized equivalent angular parameter defined as follows:

$$\psi_v = \arccos\left(\cos(\alpha_{nv}).\cos(\beta_v) - \mu_v.\sin(\beta_v)\right) \quad (2)$$

The distributed loads F_v are unknown and have to be determined with respect to all compliances. Thus, $2N_c$ loads normal to contact have to be found, meaning that $2N_c$ equations need to be written. After solving that set of equations, it will be possible to compute the load distribution in the system, i.e., the load distribution issue in the PRS. Note that the loading rate l_v on a thread can be defined as the ratio between a thread axial load and the external load referred to a roller, expressed as a percentage as defined in the following equation:

$$l_v = \frac{F_v\cos(\psi_v)}{\left(\frac{F}{n_r}\right)} \quad (3)$$

3.2 Hybrid Model of the PRS. In the present hybrid model, the different components of the PRS are represented with a series of 1D FE having two degrees-of-freedom (DOFs). These elements are bar, beam, and spring elements. The reason for using this type of element is that it is easier to encode than two-dimensional or three-dimensional FEs. Also, this approach significantly reduces the size

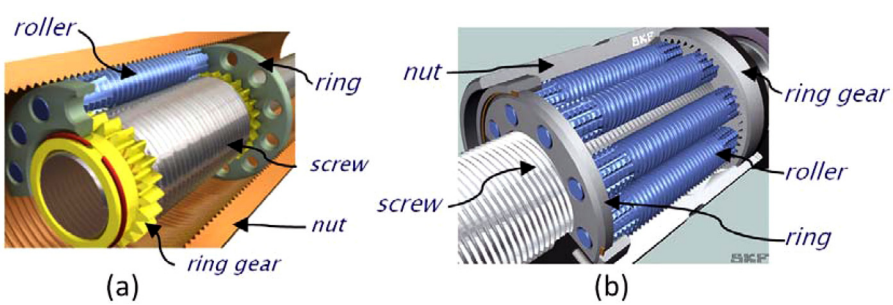

Fig. 1 (*a*) Inverted PRS and (*b*) standard PRS [15]

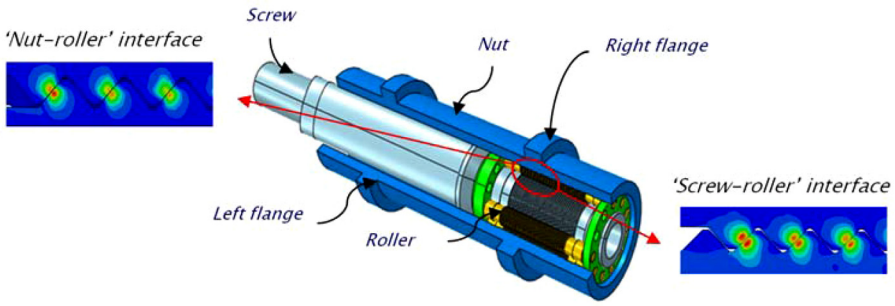

Fig. 2 Studied inverted PRS with two flanges at its initial position

of the problem, and the corresponding in-plane model is referred to as a one-dimensional finite element model (1D FEM) in this paper.

Each element describes a part of a component. Each node of the element denotes the center of the extreme section of the part. Bar elements are used to describe linear elastic behavior of the screw and the nut in the axial direction. Beam elements are used here to describe the behavior of the roller since it bends in practice. Nonlinear springs are used to model the behavior of a contact. Using a combination of these elements, the behavior of the PRS can be fully described at system level. To simplify the model, only a sector of the PRS including one complete roller is considered. The following assumptions are made:

- The ending gears of the PRS are not involved in fully axial loading.
- The roller is considered as a bending component that behaves elastically.
- The normal contact direction remains the same under loading.
- There is no friction between contacting surfaces, meaning that μ_v equals zero.
- The flexural deflection of threads is not taken into account.
- The number of contacts is assumed to be the same at each side of the roller.
- Materials are assumed to operate in their elastic range.

3.3 Meshing of Components. An appropriate choice of elements can be made only after a detailed analysis of the behavior of the system when it is subjected to loads. It is important to realize the role of each component and the issue of deformations that may affect its various sections. This analysis should be conducted from both global and local perspectives.

Usually, the nut is connected to a support assumed to be rigid. Note that the rotation of the nut generates a translation of the screw which acts on a driven component. The screw is loaded either in tension or in compression. 3D FE models [15] have shown that, for the screw, the predominant strain corresponds mainly to tension or compression. The deformations due to the bending rigidity of the threads of each component are neglected for the sake of simplicity. Thus, the screw can be considered as a bar with an annular cross-sectional area and meshed with other "bar" elements (Fig. 3). Each element represents a portion of the screw and its length is equal to the axial pitch of the screw. Using a rigid element, each contacting point or node is connected to a node of the bar element. This means that the displacements of the contact nodes derive from those of the bar elements.

The nut is constrained in translation from its shoulder using the bearings. The nut can be modeled as a cylindrical tube. According to the position of the screw relative to the shoulders, certain portions are either compressed or extended. The radial expansion is not taken into consideration, and the nut is meshed using a series of bar elements as in the case of the screw. Each node of the bar element is linked to the contacting point through a rigid element. The corresponding discrete model of the nut is shown in Fig. 3 according to the external load direction on the shaft.

Set between the screw and the nut, the roller is under contacting loads that tend to extend, compress, or bend it according to the BCs. Since the bending behavior is targeted in the present paper, the roller can be meshed with beam elements (Fig. 3).

The threaded lengths of the components are meshed with as many elements as there are contact nodes. As a result, the length of each element is equal to the axial pitch p_x, which is the same for the nut, the roller, and the screw. Any nonthreaded portion is described by an element having a length equal to the portion described here. However, for the nut, fully threaded here, any nonfunctional threaded portion that does not interact directly with other threads of the roller is modeled by one or more bar elements with the appropriate characteristics depending on the presence or absence of a flange.

By bringing together the various FEs used to mesh the various slices of the screw, the nut, and the roller, a discrete assembly can be built (Fig. 4). To model the interactions between the threads,

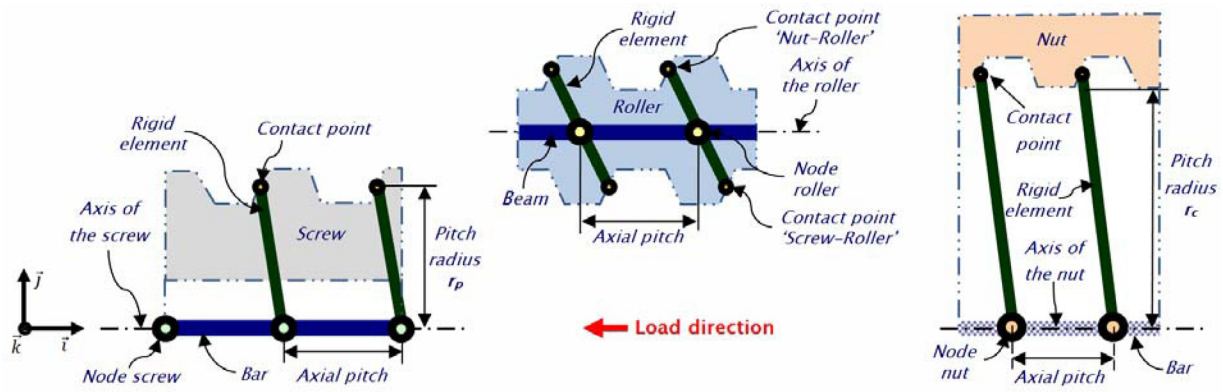

Fig. 3 Discrete model of components of the inverted PRS

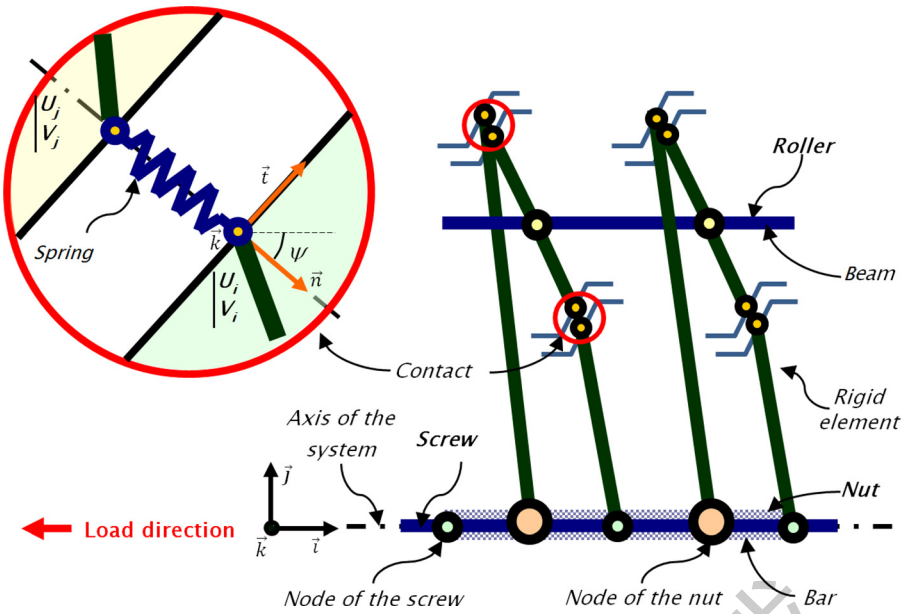

Fig. 4 Discrete model of the PRS mechanism

nonlinear springs are used in the direction ψ_v or $(\pi-\psi_v)$ according to the external compressive or tensile force in the axial plane.

3.4 Interaction Laws. The springs used to describe the contact between threads are nonlinear in order to correctly model the deflection of the centers of the contacting flanks. This deflection is due to the nonlinear local deformations at the interface of a pair of flanks under a contacting load, which is an unknown distributed load. Moreover, it is assumed that the springs act only in the direction normal to the flanks. That direction is also considered invariable under a given load, and the springs are only active when compressed. The parameters k_o of these springs were identified from the contacting surfaces' characteristics (contact radii, surfaces curvatures, and Young's modulus) using Hertzian theory [15,16].

In the local coordinates system, the ending nodes i and j (Fig. 4) of the spring elements are characterized by the DOFs w_i and w_j, respectively, corresponding to nodal displacements $u_i = f_i(w_i)$, $v_i = g_i(w_i)$ for node i and to $u_j = f_j(w_j)$, $v_j = g_j(w_j)$ for node j in the global basis. Note that the nodal displacements are based on w_i and w_j. In the global basis, the stiffness matrix $\mathbf{K}_S$ related to the nodal displacements u_i and v_i of the node i and nodal displacements u_j and v_j of the node j is given by the following equation:

$$K_s = k_v \cdot T_b{}^t(\psi_v) \cdot [K_{\text{be}}] \cdot T_b(\psi_v) \tag{4}$$

where matrices T_b and K_{be} are defined in the Appendix, k_V is the nonlinear elasticity of the contact or of the spring given by the following equation:

$$k_v = \frac{1}{(\cos\psi_v)^n} k_0 (u_i - u_j)^{n-1} = \frac{1}{(\sin\psi_v)^n} k_0 (v_i - v_j)^{n-1} \tag{5}$$

where n is a constant of value 2/3, k_0 is the elastic modulus, which depends on material and geometric properties: radii of curvature, Young's modulus, Poisson's ratio, etc.

The stiffness matrix $\mathbf{K}_S$ of the spring can finally be written according to Eq. (6). The matrix $\mathbf{K}_S$ is obviously not linear due to $\mathbf{K}_V$, which is a nonlinear function based on the nodal displacements u_i, u_j or v_i, v_j

$$K_s = \frac{1}{(\cos\psi_v)^n} k_0 (u_i - u_j)^{n-1} \cdot T_b{}^t(\psi_v) \cdot [K_{\text{be}}] \cdot T_b(\psi_v) \tag{6}$$

3.5 Global Stiffness Matrix of the System. The stiffness matrices $\mathbf{K}_V$ and $\mathbf{K}_D$ of the screw and the nut, respectively, can be obtained using the elementary matrix $\mathbf{K}_b$ of a bar element. The stiffness matrix $\mathbf{K}_{\text{Ro}}$ of the roller is derived by assembling the elementary matrix $\mathbf{K}_p$ of a beam element. Also, after adding the elementary matrix $\mathbf{K}_S$ of each spring, the nonlinear matrix $\mathbf{K}_{\text{Sp}}$ of the "super-element" denoted "multisprings" can be constructed. The elementary matrices $\mathbf{K}_b$, $\mathbf{K}_p$, and $\mathbf{K}_S$ are given in the Appendix. The global stiffness matrix $\mathbf{K}_n$ of the PRS is expressed by Eq. (7), where $\mathbf{q}_{nd}$ is the vector of DOFs of the nodes of the contacting springs

$$K_n = \text{diag}\begin{pmatrix} K_V \\ K_D \\ K_{\text{Ro}} \\ K_{\text{Sp}}(\{q_{nd}\}) \end{pmatrix} \tag{7}$$

3.6 BCs. It is important to set the BCs applied to the system in terms of loading and displacements. Four BCs have been identified (BC1, BC2, BC3, and BC4).

BC1: since, in practice, it is assumed that the screw undergoes pure axial deformation, all the radial displacements of the bar element are zero. The figure below (Fig. 5) illustrates the BCs applied to the screw shaft. For easier comprehension, the rigid elements are not represented. This BC is expressed by the relation of Eq. (8), where p is the number of nodes used to mesh the screw shaft

$$v_1 = \cdots = v_p = 0 \tag{8}$$

BC2: as the screw shaft is under a load F_0, its left node is constrained. The external force F_0 is applied in the negative sense for the tensile case (TC) and in the positive sense for the compressive case (CC). This load BC is set by operating on the vector of nodal external forces $\mathbf{F}_n$. This BC is expressed by the following equation:

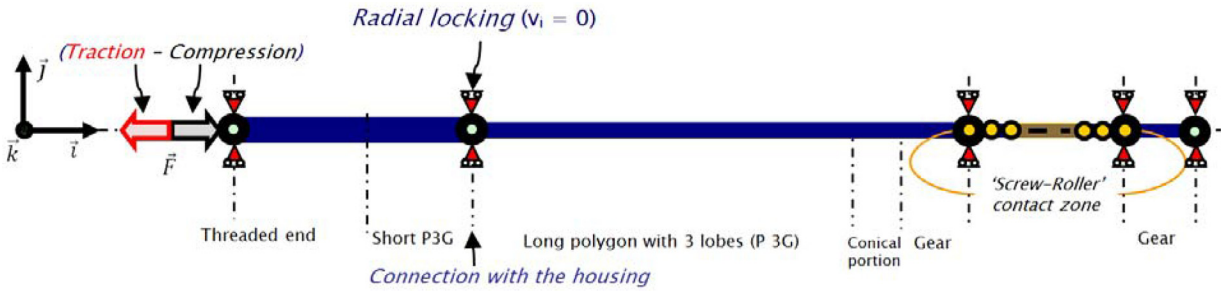

Fig. 5 BCs on the screw without the representation of the corresponding rigid elements

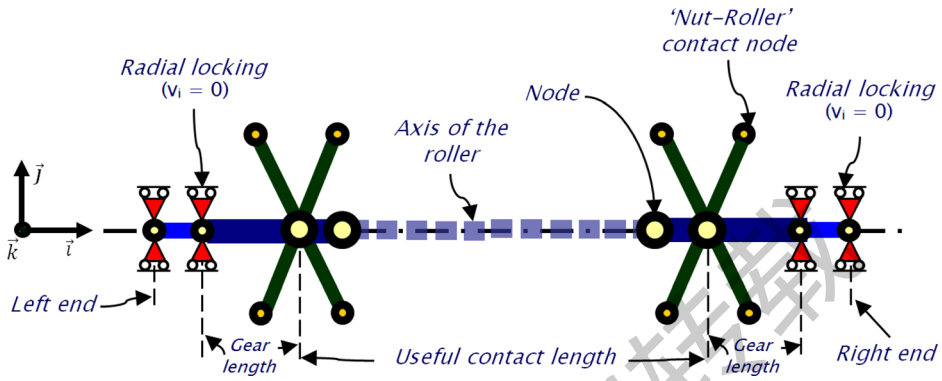

Fig. 6 BCs on the roller

$$\{F_n\} = \{F_0 \quad \dots \quad \dots \quad 0\}^t \tag{9}$$

BC3: the presence of the two rings is modeled through the application of two constraints on each end of the roller as shown in Fig. 6. It is assumed that the radial displacement at each end is zero for a roller. In that case, the BC is represented by Eq. (10), where q corresponds to the number of nodes used to mesh the roller and g corresponds to the total number of nodes used to mesh both the screw and the nut

$$v_{p+1} = v_{p+2} = v_{p+q-1} = v_{p+q} = 0 \tag{10}$$

BC4: for the nut, all the radial displacements of the nodes are zero as for the screw shaft. In addition, the node representing the "thrust" near the section of the blocked flange is constrained axially in motion. Its displacement is set to zero as described by the following equations:

$$u_c = 0 \tag{11}$$

$$v_{p+1} = \cdots = v_{p+q} = \cdots = v_{p+g-1} = \cdots = v_{p+q+g} = 0 \tag{12}$$

3.7 Configurations of the System. To address these problems, three main configurations of the PRS under study that fit the possible relative positions of the screw shaft according to the nut and the thrust are identified. The figures below (Figs. 7–9) illustrate these configurations in a simplified way by focusing on the representation of the nut without the rigid elements or the symbols of BCs. Nevertheless, the node axially constrained in motion is clearly indicated: at left for the TC and at right for the CC. Other intermediate configurations are available in Ref. [15].

It is important to distinguish such configurations in order to construct the stiffness matrices of the nut as the number of element changes depending on the configuration. The distinction is also important for the determination of the subscript or the rank of the node corresponding to the thrust, since that subscript depends on the configuration of the system and the type of loading (compressive or tensile).

CONFIG 1 is the configuration where the system is at its initial position. CONFIG 2 is the configuration where the set of rollers and the screw are in the middle of the nut. CONFIG 3 is the configuration where the screw reaches its final position.

3.8 Numerical Solution of the Problem. The resolution of the problem is based on an energy formulation. It takes advantage of dependency relationships between displacements due to rigid coupling elements. The derivative of the total potential energy E_{PT} of the system is as expressed by the following equation:

$$\frac{\partial}{\partial q_j}(E_{PT}) = 0 \tag{13}$$

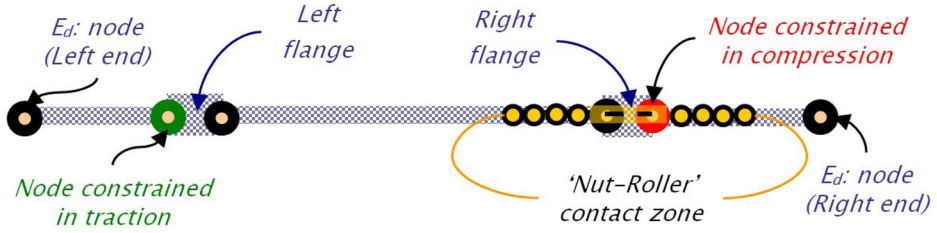

Fig. 7 Meshing of the nut in CONFIG 1

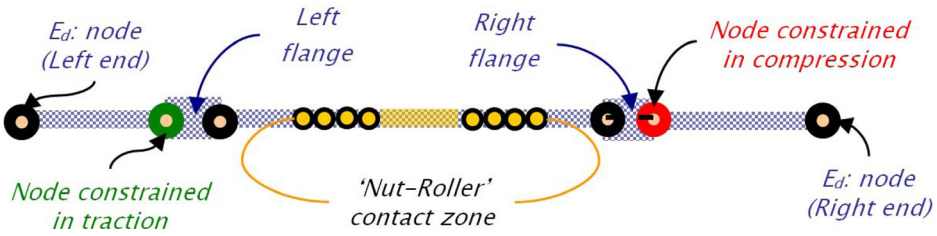

Fig. 8 Meshing of the nut in CONFIG 2

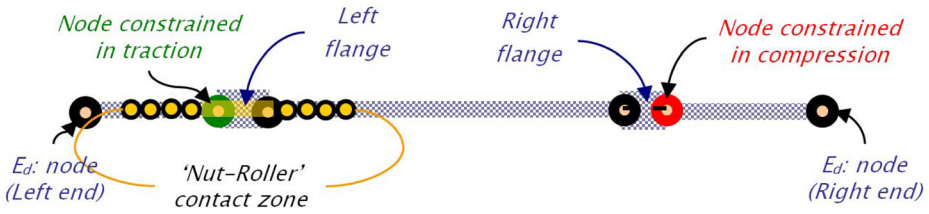

Fig. 9 Meshing of the nut in CONFIG 3

where the potential energy E_{PT} is given by Eq. (14), with $\{\mathbf{q}_n\}$ the vector of DOFs of all nodes including those of springs

$$E_{PT} = \frac{1}{2}\{q_n\}^t \cdot [K_n] \cdot \{q_n\} - \{q_n\}^t \cdot \{F_n\} \tag{14}$$

The vector $\mathbf{q}_n$ can be rewritten based on the DOFs $\mathbf{q}_{ni}$ of the nodes describing the components as shown by the following equation:

$$\{q_n\} = \begin{Bmatrix} q_{ni} \\ q_{nd} \end{Bmatrix} = \begin{bmatrix} I \\ G_{di} \end{bmatrix} \cdot \{q_{ni}\} \tag{15}$$

where $\mathbf{I}$ is the identity matrix, $\mathbf{G_{di}}$ is the adjacency matrix that connects $\mathbf{q}_{nd}$, the DOFs of the nodes of the contacting springs, to $\mathbf{q}_{ni}$, the DOFs of the components' nodes. The adjacency matrix $\mathbf{G_{di}}$ can be found in Ref. [15]. Thanks to Eq. (15), the expression of the potential energy E_{PT}, Eq. (14), yields the relation of the following equation:

$$E_{PT} = \frac{1}{2}\{q_{ni}\}^t \cdot [K_R] \cdot \{q_{ni}\} - \{q_{ni}\}^t \cdot \{F_R\} \tag{16}$$

where $\mathbf{K}_R$ and $\mathbf{F}_R$, given by Eqs. (17) and (18), are, respectively, the reduced stiffness matrix of the system and the reduced vector of nodal forces

$$[K_R] = \begin{bmatrix} I & G_{di}^{\mathrm{T}} \end{bmatrix} \cdot [K_n] \cdot \begin{bmatrix} I \\ G_{di} \end{bmatrix} \tag{17}$$

$$\{F_R\} = \begin{bmatrix} I & G_{di}^{\mathrm{T}} \end{bmatrix} \cdot \{F_n\} \tag{18}$$

Table 1 Parameters of the inverted PRS

Parameters	Symbols	Units	Values
Pitch diameter of the screw	d_s	mm	21
Lead	p_z	mm	5
Number of starts	n_s	—	3
Number of rollers	n_r	—	11
Number of contacts at each interface	N_c	—	20
Pressure angle	α_n	deg	45
Maximum external load	F	kN	45
Static load capacity	C_{a0}	kN	91.8
Young's modulus	E	GPa	209

The nodal displacements stored in the vector $\mathbf{q}_{ni}$ are unknown and must be determined by solving the nonlinear set of reduced equations, Eq. (19)

$$[K_R] \cdot \{q_{ni}\} = \{F_R\} \tag{19}$$

To solve Eq. (19), either the Newton–Raphson method or the Fixed Point method can be used, both of which are iterative techniques. Once the nodal displacements $\mathbf{q}_{ni}$ are known, the nodal displacements $\mathbf{q}_{nd}$ of the springs can be computed using the following equation:

$$\{q_{nd}\} = [G_{di}] \cdot \{q_{ni}\} \tag{20}$$

Finally, the distributed loads F_v can easily be computed using the stiffnesses of the springs as given by Eq. (21) and calculating the loading rates l_V with Eq. (3)

$$F_v = \frac{1}{(\cos\psi_v)^n} k_0 (u_i - u_j)^n = k_v \cdot (u_i - u_j) \tag{21}$$

4 Application and Results

As an example of application, an inverted PRS is considered with a maximum load applied to the screw shaft that represents 50% of the static load capacity, C_{a0}, of the mechanism. It is assumed that the number of contacts is the same at each side of a roller. All the input parameters of the inverted PRS are summarized in Table 1. The nonlinear contact parameters are derived and summarized in Table 2. Let us compare the results (Figs. 10–14) obtained from our model and those from a 3D FE model, which is considered as the reference. The BCs are the same for the two models and the comparison is made in the three configurations (CONFIG 1, CONFIG 2, and CONFIG 3).

4.1 Axial Stiffness of the PRS. The axial stiffnesses in the three configurations are illustrated by Fig. 12. The stiffnesses computed by our model are in good agreement with those from the 3D FEM. The maximum relative discrepancies are −9% (TC) and 4% (CC) in CONFIG 1, 3% (TC) and −9% (CC) in CONFIG 2, and −5% (TC) and 7% (CC) in CONFIG 3. It can be observed that the axial stiffness depends on the configuration of the mechanism and the loading direction. In the present case of the inverted PRS, while the screw shaft is moving inside, the axial stiffness

Table 2 Parameters at contacting interfaces

Parameters	Symbols	Units	Values
Generalized angular parameter at the screw–roller interface	ψ_k	deg	45.0288
Generalized angular parameter at the nut–roller interface	ψ_g	deg	45.0803
Equivalent curvature radius at screw–roller interface	R_{qk}	mm	2.4846
Equivalent curvature radius at nut–roller interface	R_{qg}	mm	1.9610
Constant elasticity at screw–roller interface	k_{ok}	$\mathrm{N \cdot mm^{-3/2}}$	3.6062×10^5
Constant elasticity at nut–roller interface	k_{og}	$\mathrm{N \cdot mm^{-3/2}}$	4.2140×10^5

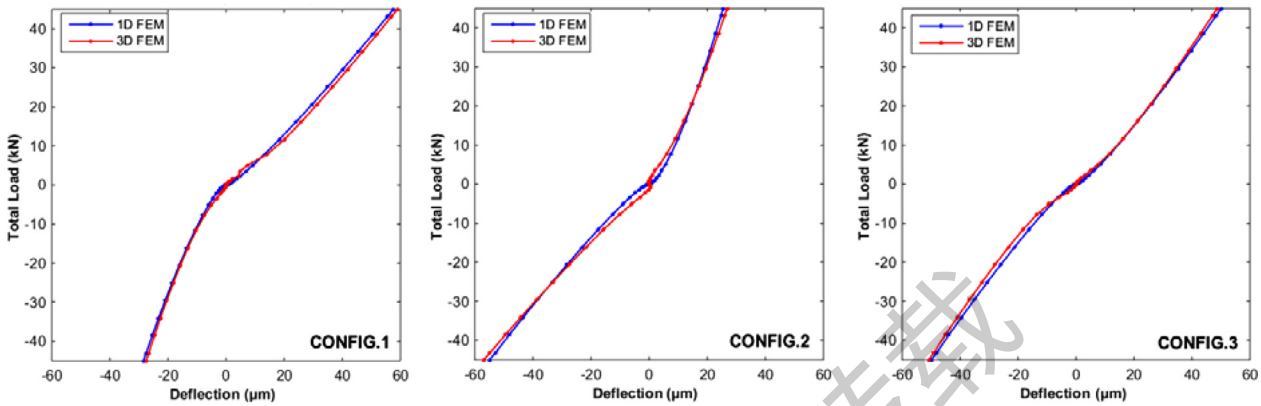

Fig. 10 Axial stiffness curves in CONFIGs 1, 2, and 3 with a bending flexible roller

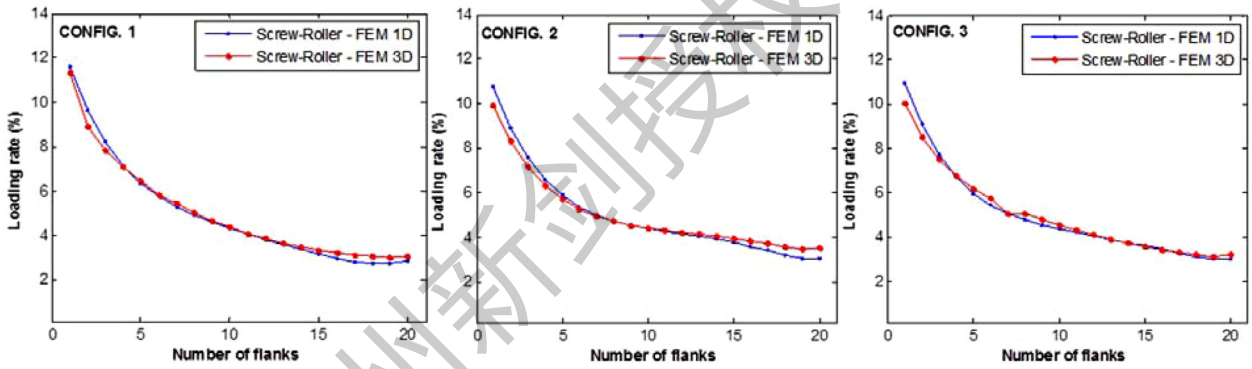

Fig. 11 Load distribution at the screw–roller side in a CC in CONFIGs 1, 2, and 3

increases under tensile loading and decreases under compressive loading.

4.2 Load Distribution at the Screw–Roller Interface. At the "screw–roller" interface, the load distribution varies according to the system configuration and the loading direction. The most critical situation for the threads of the screw appears to be compressive loading. This is mainly due to the effect of the roller's flexibility. In all configurations, the load decreases from the first thread of the screw to the last. Also, the predictions of the hybrid

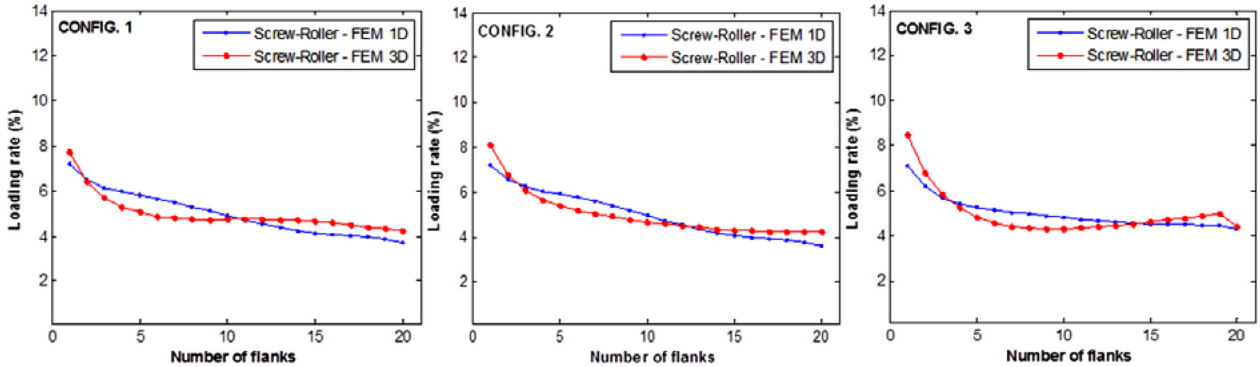

Fig. 12 Load distribution at the screw–roller side in a TC in CONFIGs 1, 2, and 3

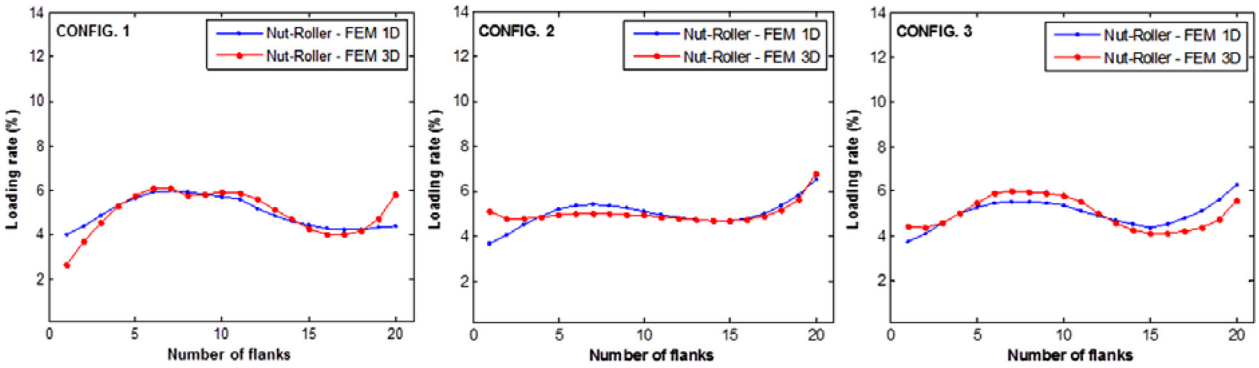

Fig. 13 Load distribution at the nut–roller side in a CC in CONFIGs 1, 2, and 3

model are in good agreement with the 3D FEM incorporating a flexible roller.

In the CC, the model underpredicts the loading rates with respect to the reference model for some threads and overpredicts for others (Fig. 11). The highest discrepancy is about 10.2% and the lowest is about −9%. The mean of the relative discrepancies is less than 3% in any of the three configurations. In the TC, the model captures the global tendency well and is also in quite good agreement with the reference model (Fig. 12). The differences between the two models are slightly greater than in the CC. The highest relative gap is about 15.9% and the lowest is about −15.6%, whereas the mean of the relative discrepancies is less than 2% in each configuration.

4.3 Load Distribution at the Nut–Roller Interface. At the nut–roller interface, the load distribution differs greatly from one configuration to another. It depends on the loading case, the flexibility of the roller, the position of the nut's flanges, and the thrust. The effect of the flange on the load distribution is evaluated with more or less accuracy.

The model predicts results in the CC well, in comparison with the 3D FEM analysis (Fig. 13). The highest relative discrepancy is about 28.2% and the lowest is about −52%. The mean relative discrepancies are −2.1% in CONFIG 1, −0.3% in CONFIG 2, and −0.9% in CONFIG 3.

Results computed in the TC do not fully agree with those of the FEM analysis (Fig. 14). The highest relative discrepancy is about 29.3%, the lowest is about −36.8%. Nevertheless, the mean discrepancies are 3.8% in CONFIG 1, 4.3% in CONFIG 2, and 1.9% in CONFIG 3. It can be noted that the effect of the flanges or thrust is not well captured. Though the model underestimates or overestimates results, the global trend is quite similar. This means that the flexibility of the roller is overestimated in our model comparatively to the 3D FEM. The reason is that in our model the deformation of the threads is neglected and the contact direction is assumed not to vary under loading. Also, it must be pointed out that the load ratio on the first thread is higher than that computed in the CC.

5 Discussion

As noted above, the results of the load distribution are in quite good agreement for the screw–roller contacts and are slightly different for the nut–roller contacts, though the global tendency is qualitatively well reproduced with respect to the reference model. The disturbance induced in the area of the thrust and flanges is well reflected by our hybrid model at the nut–roller interface in the CC but not in the tensile one. The discrepancies between the two models at the nut side may be due to the fact that the radial expansions of components and even the flexural deflection of threads are neglected in the hybrid model. All this demonstrates how difficult the topic of load distribution in the PRS is, especially when the arbitrary shape of the nut must be taken into account. Since the current model is almost efficient, it can be used for a parametric study. For instance, it is possible to check whether or not the load distribution is depended on the external load applied to the screw shaft.

Next, the load distribution is computed when varying the external load in the three main configurations. The purpose is to see whether and how the load distribution depends on the external load applied. Figures 15–18 plot the load distribution versus the external load applied to the screw shaft for both nonflexible and flexible rollers. As shown by those figures, the load distribution can be described as "butterfly wings." The red curve relates to the first thread, the blue to the second, and the green to the last, the black curves corresponding to the 17 remaining or intermediate threads. Considering any external load, it can be seen that the sum of the distributed loading rates is equal to 100%. For lower external loads, the load distribution is quite uniform as the loading rate on each thread is around 5% (the average) in both tensile and CCs at the nut–roller and the screw–roller interfaces. Regardless of the

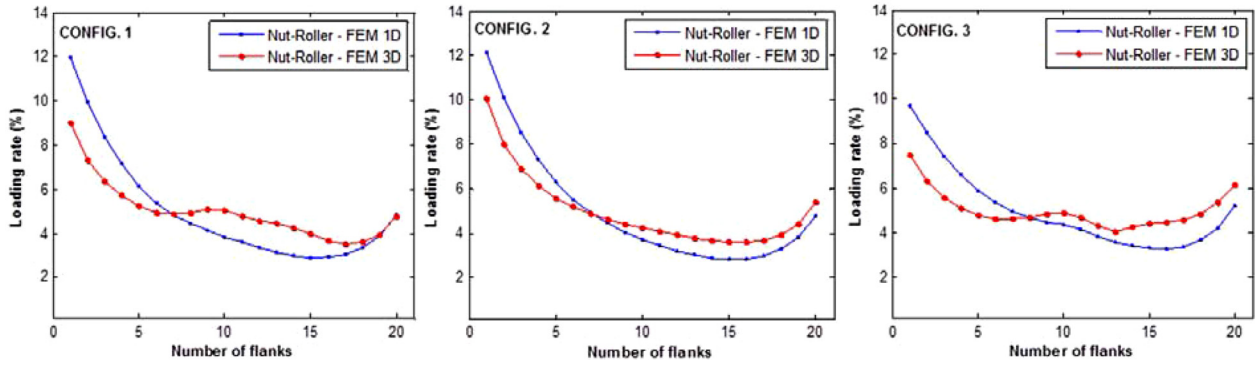

Fig. 14 Load distribution at the nut–roller side in a TC in CONFIGs 1, 2, and 3 for a bending flexible roller

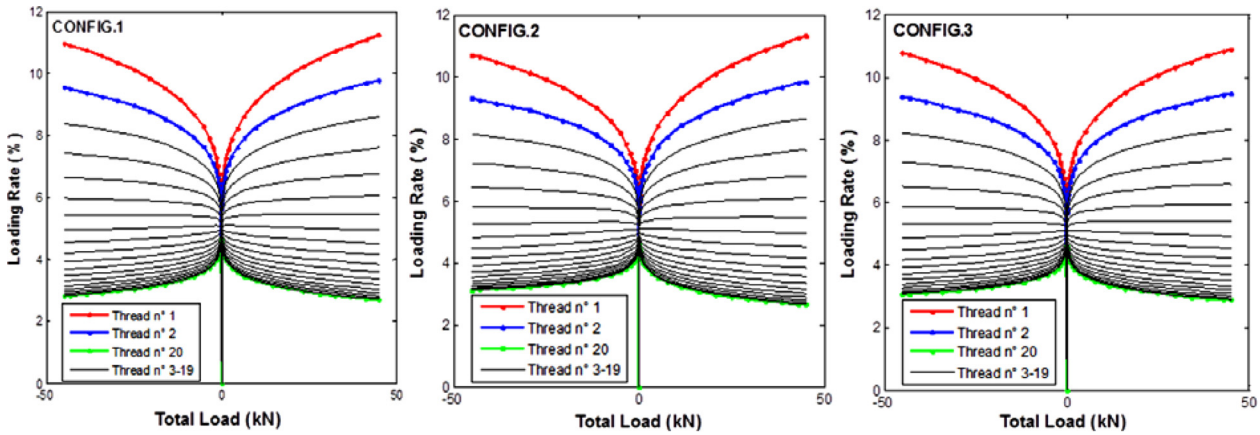

Fig. 15 Load distribution against the external load at screw–roller interface in CONFIGs 1, 2, and 3 for a nonflexible roller

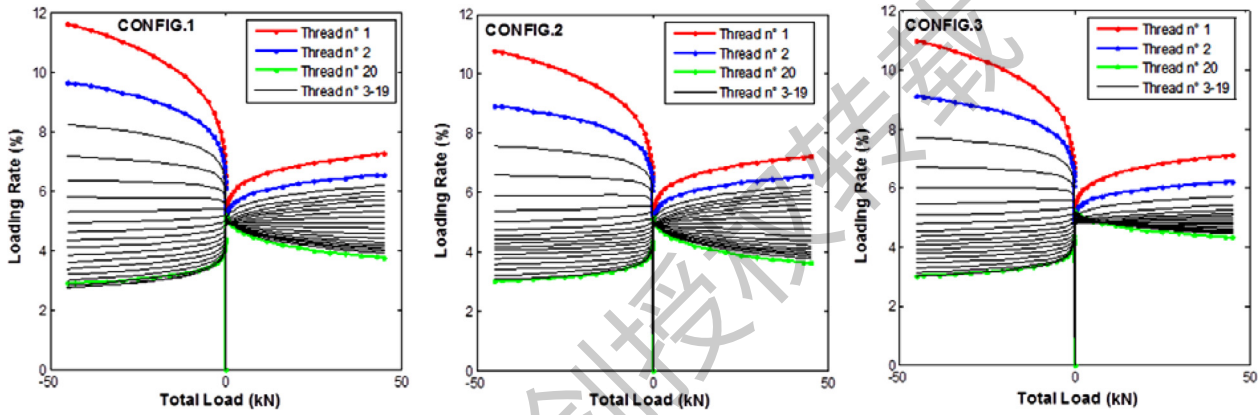

Fig. 16 Load distribution against the external load at screw–roller interface in CONFIGs 1, 2, and 3 for a bending flexible roller

loading direction, when the external load increases, each loading rate evolves in such a way that the global load distribution becomes nonuniform or gradual.

Furthermore, the load distribution depends on the external load and reveals that the first active thread of the screw shaft is the most loaded one in any configuration as its load ratio is the highest. The load ratio increases with the external loading on the shaft and is similar in all identified configurations. Since the load ratios of the first six threads increase with the external load, the load ratios of the last ten threads decrease.

The flexibility of the roller also influences the load distribution for the nut–roller contacts as well as for the screw–roller contacts, since the butterfly wings are not the same as the previous ones in the case of a nonflexible roller. The left "wing" is more split or

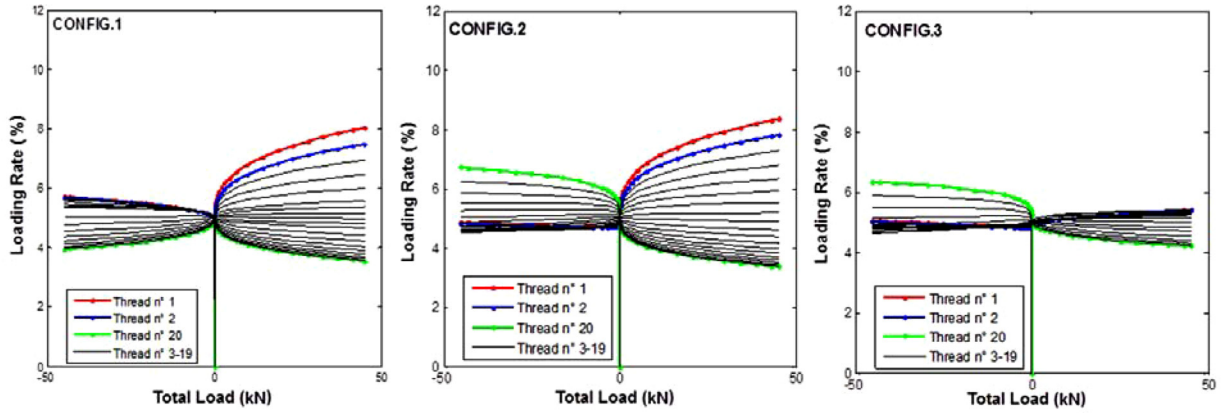

Fig. 17 Load distribution against the external load at nut–roller interface in CONFIGs 1, 2, and 3 for a nonflexible roller

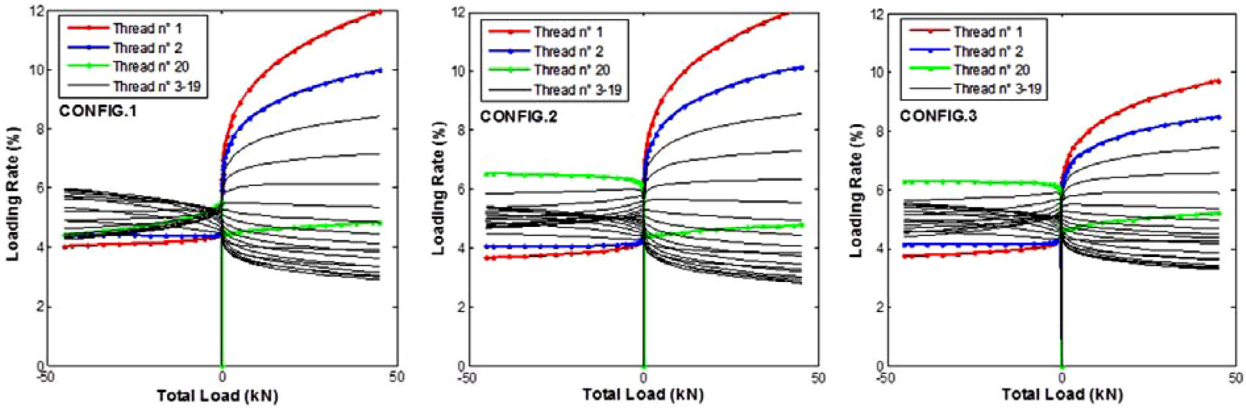

Fig. 18 Load distribution against the external load at nut–roller interface in CONFIGs 1, 2, and 3 for a bending flexible roller

larger under tensile loading than under compressive loading. This means that the load distribution is more sensitive to the flexibility of the roller in the first loading case than in the second. For the screw, the load on the first thread increases slightly in the TC whereas, in the CC, it is reduced by about 40% with a nonflexible roller. For the nut, in the TC, the first active thread remains the most loaded whether the roller is flexible or not. The load ratio on the first active thread is almost 1.5 times higher in the flexible roller case than with the nonflexible roller. In the compressive loading case, the position of the most loaded thread depends strongly on the system configuration and the flexibility of the roller.

6 Conclusion

The objective of this paper has been to present a hybrid model based on the use of bar, beam, and nonlinear spring elements to represent a PRS mechanism in order to compute its load distribution and its axial stiffness under static loading. The model has the advantage of involving the axial elasticity of the roller and its bending flexibility under compressive or tensile loading. The current model gives good predictions of the axial stiffness and the load distribution at each side of the roller in different configurations even if the load sharing related to the nut–roller interface could be optimized. It has been shown that the shape of the nut has a notable influence on the load distribution as its flanges interact with the contacting threads. Under compressive loading, the flexibility of the roller has little impact on the load distribution whereas, under tensile loading, it completely modifies the load distribution. Also, the BCs have a strong influence on both the load distribution and the axial stiffness of the mechanism.

A parametric study demonstrated that the load distribution was not unique but was different at each interface of the roller. The load distribution is sensitive to the loading cases (tensile or compressive) and depends greatly on the external loading value applied to the screw shaft as well as on the type of configuration related to the flanged nut. It is also sensitive to whether the roller behaves as a pure elastic or a flexible component. Although the example studied here is limited to an inverted PRS, the presented approach has been extended to a "standard" PRS for validation. This model finally appears to be a reliable alternative to 3D FE analysis and could be used to better understand the static behavior of PRSs by studying the distribution of pressures and stresses.

This hybrid model has been developed for a lifetime calculation tool to analyze thousands of loading cycles from an aircraft flight data collection, which have been previously reduced by a "rainflow" approach. In these circumstances, it is not possible to rely on sophisticated 3D FE models as the calculation times become prohibitive. Thus, it is essential to have a sufficiently reliable tool available that gives almost instantaneous results so that choices of designs or architectures can be made quickly and easily with regard to a preliminary product development phase of any PRS. Also, this hybrid model is relevant enough and efficiently exploitable to study the influence of parameters based on a design of experiment.

Acknowledgment

The authors are deeply grateful to the SKF Company for its grant and support. This work was performed under a Ph.D. dissertation contract at INSA de Toulouse, France.

Nomenclature

C_{a0} = static load capacity
C_v = screw–roller or nut–roller contact
d_s = pitch diameter of the screw
E = Young's modulus of all materials
E_b = Young's modulus related to a bar element
E_{PT} = total potential energy of the system
F = axial external force acting upon the central screw shaft
$\mathbf{F}_n$ = vector of external forces applied to the whole system
$\mathbf{F}_R$ = reduced nodal external forces
F_0 = nodal force applied to the shaft
$\mathbf{G}_{di}$ = adjacency matrix
$\mathbf{I}$ = identity matrix
k, g = subscripts referring to screw–roller and "nut–roller" contacts, respectively
k_v = nonlinear stiffness of a spring
k_0 = elasticity constant defining a Hertzian contact
k_{0g} = elasticity constant for a screw–roller contact
k_{0k} = elasticity constant for a nut–roller contact
$\mathbf{K}_b$ = elementary stiffness matrix of a bar element in the global basis
$\mathbf{K}_{be}$ = elementary stiffness matrix of a bar element in the local basis
$\mathbf{K}_D$ = stiffness matrix of the nut
$\mathbf{K}_n$ = nonlinear global stiffness of the system
$\mathbf{K}_p$ = elementary stiffness matrix of a beam element in the global basis
$\mathbf{K}_{pe}$ = elementary stiffness matrix of a beam element in the local basis
$\mathbf{K}_R$ = reduced global stiffness of the system
$\mathbf{K}_{Ro}$ = stiffness matrix of the roller
$\mathbf{K}_S$ = stiffness matrix associated with a spring in the global basis
$\mathbf{K}_{Sp}$ = stiffness matrix of the multisprings

$\mathbf{K}_V$ = stiffness matrix of the screw shaft
l_b = length of a bar element
l_p = length of a beam element
l_v = loading rate
n = constant of value 2/3
n_r = number of rollers
n_s = number of starts
N_c = number of contacts
p = number of nodes used to discretized the screw shaft
p_x = axial pitch
p_z = lead of the screw
$\mathbf{q}_n$ = vector of DOF of all nodes of the discrete PRS
$\mathbf{q}_{nd}$ = vector of DOF related to the nodes of the springs
$\mathbf{q}_{ni}$ = vector of DOF related to the nodes of components
R_{qg} = equivalent curvature radius at nut–roller interface
R_{qk} = equivalent curvature radius at screw–roller interface
S_b = section related to a bar element
S_p = section related to a beam element
$\mathbf{T}_b$ = transformation matrix from local basis to global coordinates system
$\mathbf{T}_p$ = transformation matrix from local basis to global coordinates system for a beam element
u_c = nodal displacement of the fixed node of the nut
u_i, u_j = axial nodal displacement of a spring in the global basis
v = subscript that represents k or g
v_i, v_j = radial nodal displacement of a spring in the global basis
v_p, v_g = subscripts referencing nodes on which BCs are set
w_i, w_j = nodal displacement of a spring in the local basis
α_{nv} = pressure angle
β_v = lead angle of the screw or the nut
μ_v = friction coefficient at screw–roller or nut–roller interfaces
ϕ_b = angular deviation between the local and the global coordinate systems
ϕ_p = angular deviation between the local and the global coordinates systems for a beam element
ψ_g = generalized angular parameter for a spring at a nut–roller interface
ψ_k = generalized angular parameter for a spring at a screw–roller interface
ψ_v = generalized angular parameter for a spring at a contacting interface

Appendix

Elementary stiffness matrix of the bar in the local coordinates system

$$K_{\text{be}} = \frac{E_b S_b}{l_b}\begin{bmatrix} 1 & 0 & -1 & 0 \\ 0 & 0 & 0 & 0 \\ -1 & 0 & 1 & 0 \\ 0 & 0 & 0 & 0 \end{bmatrix} \tag{A1}$$

Stiffness matrix $\mathbf{K}_b$ in the global coordinates system

$$K_b = T_b'(\phi_b) \cdot [K_{\text{be}}] \cdot T_b(\phi_b) \tag{A2}$$

The transformation matrix $\mathbf{T}_b$ from the local basis to global coordinates system

$$T_b(\phi_b) = \begin{bmatrix} \cos\phi_b & \sin\phi_b & 0 & 0 \\ -\sin\phi_b & \cos\phi_b & 0 & 0 \\ 0 & 0 & \cos\phi_b & \sin\phi_b \\ 0 & 0 & -\sin\phi_b & \cos\phi_b \end{bmatrix} \tag{A3}$$

Elementary stiffness matrix $\mathbf{K}_{pe}$ of the beam in the local coordinates system

$$K_{pe} = \begin{bmatrix} \frac{E_p S_p}{l_p} & 0 & 0 & -\frac{E_p S_p}{l_p} & 0 & 0 \\ 0 & \frac{12E_pI_p}{l_p^3} & \frac{6E_pI_p}{l_p^2} & 0 & -\frac{12E_pI_p}{l_p^3} & \frac{6E_pI_p}{l_p^2} \\ 0 & \frac{6E_pI_p}{l_p^2} & \frac{4E_pI_p}{l_p} & 0 & -\frac{6E_pI_p}{l_p^2} & \frac{2E_pI_p}{l_p} \\ -\frac{E_p S_p}{l_p} & 0 & 0 & \frac{E_p S_p}{l_p} & 0 & 0 \\ 0 & -\frac{12E_pI_p}{l_p^3} & -\frac{6E_pI_p}{l_p^2} & 0 & \frac{12E_pI_p}{l_p^3} & -\frac{6E_pI_p}{l_p^2} \\ 0 & -\frac{6E_pI_p}{l_p^2} & \frac{2E_pI_p}{l_p} & 0 & -\frac{6E_pI_p}{l_p^2} & \frac{4E_pI_p}{l_p} \end{bmatrix} \tag{A4}$$

Stiffness matrix $\mathbf{K}_p$ of the beam element, in the global coordinates system

$$K_p = T_p{}^t(\phi_p) \cdot [K_{pe}] \cdot T_p(\phi_p) \tag{A5}$$

Matrix $\mathbf{T}_p$ for transformation from the local coordinates system to the global coordinates system

$$T_p(\phi_p) = \begin{bmatrix} \cos\phi_p & \sin\phi_p & 0 & 0 & 0 & 0 \\ -\sin\phi_p & \cos\phi_p & 0 & 0 & 0 & 0 \\ 0 & 0 & 1 & 0 & 0 & 0 \\ 0 & 0 & 0 & \cos\phi_p & \sin\phi_p & 0 \\ 0 & 0 & 0 & -\sin\phi_p & \cos\phi_p & 0 \\ 0 & 0 & 0 & 0 & 0 & 1 \end{bmatrix} \tag{A6}$$

References

[1] Otsuka, J., Fukada, S., and Osawa, T., 1987, "Fundamental Study of Planetary Screw-Structure and Coefficient of Friction," Bull. Jpn. Soc. Precis. Eng., **21**(1), pp. 43–48.
[2] Otsuka, J., Osawa, T., and Fukada, S., 1989, "A Study on the Planetary Roller Screw. Comparison of Static Stiffness and Vibration Characteristics With Those of the Ball Screw," Bull. Jpn. Soc. Precis. Eng., **23**(3), pp. 217–223.
[3] Lemor, P. C., 1996, "The Roller Screw, an Efficient and Reliable Mechanical Component of Electromechanical Actuators," British Library—The Worlds Knowledge, 31st International Energy Conversion Engineering Conference (IECEC 96), Washington, DC, Aug. 11–16, Vol. 1, pp. 215–220.
[4] Tselishchev, A. S., and Zharov, I. S., 2008, "Elastic Elements in Roller-Screw Mechanisms," Russ. Eng. Res., **28**(11), pp. 1040–1043.
[5] Hojat, Y., and Agheli, M., 2009, "A Comprehensive Study on Capabilities and Limitations of Roller Screw With Emphasis on Slip Tendency," Mech. Mach. Theory, **44**(10), pp. 1887–1899.
[6] Velinsky, A., Chu, B., and Lasky, T. A., 2009, "Kinematics and Efficiency Analysis of the Planetary Roller Screw Mechanism," ASME J. Mech. Des., **131**(1), p. 011016.
[7] Jones, M. H., and Velinsky, A., 2012, "Kinematics of Roller Migration in the Planetary Roller Screw Mechanism," ASME J. Mech. Des., **134**(6), p. 061006.
[8] Jones, M. H., and Velinsky, A., 2013, "Contact Kinematics in the Roller Screw Mechanism," ASME J. Mech. Des., **135**(5), p. 051003.
[9] Liu, Y., and Wang, J., 2014, "Simulation of a Crossing Threaded Planetary Roller Screw Engagement," Adv. Mater. Res., **889–890**, pp. 518–526.
[10] Shangjun, M., Geng, L., Jianxing, Z., and Ruiting, T., 2011, "Optimal Design and Contact Analysis for Planetary Roller Screw," Appl. Mech. Mater., **86**, pp. 361–364.
[11] Shangjun, M., Geng, L., Ruiting, T., and Xiaocai, Z., 2012, "A New Study on the Parameter Relationships of Planetary Roller Screws," Math. Probl. Eng., **2012**, p. 340437.
[12] Xuesong, M., Masaomi, T., Tao, T., and Nuagang, S., 2003, "Study on the Load Distribution of Ball Screws With Errors," Mech. Mach. Theory, **38**(11), pp. 1257–1269.
[13] Rys, J., and Lisowski, F., 2013, "The Computational Model of the Load Distribution Between Elements in Planetary Roller Screw," J. Theoretical Appl. Mech., **82**(3), pp. 699–705.
[14] Jones, M. H., and Velinsky, A., 2014, "Stiffness of the Roller Screw Mechanism by the Direct Method," Mech. Based Des. Struct. Mach.: Int. J., **42**(1), pp. 17–34.
[15] Abevi, F. K., 2013, "Development of a Support Tool for the Preliminary Design of a Planetary Roller Screw Under Complex Loadings," Ph.D. thesis, Institut Clément ADER (ICA) of INSA de Toulouse, France, http://www.theses.fr/2013ISAT0038
[16] Johnson, L. K., 1985, *Contact Mechanics*, Cambridge University Press, Cambridge, UK.